

Electron-spin dynamics in elliptically polarized light waves

Heiko Bauke,^{1,*} Sven Ahrens,^{1,2} and Rainer Grobe^{1,2}

¹Max-Planck-Institut für Kernphysik, Saupfercheckweg 1, 69117 Heidelberg, Germany

²Intense Laser Physics Theory Unit and Department of Physics,
Illinois State University, Normal, Illinois 61790-4560 USA

(Dated: November 4, 2014)

We investigate the coupling of the spin angular momentum of light beams with elliptical polarization to the spin degree of freedom of free electrons. It is shown that this coupling, which is of similar origin as the well-known spin-orbit coupling, can lead to spin precession. The spin-precession frequency is proportional to the product of the laser-field's intensity and its spin density. The electron-spin dynamics is analyzed by employing exact numerical methods as well as time-dependent perturbation theory based on the fully relativistic Dirac equation and on the nonrelativistic Pauli equation that is amended by a relativistic correction that accounts for the light's spin density.

PACS numbers: 03.65.Pm, 31.15.aj, 31.30.J-

1. Introduction

Novel light sources such as the ELI-Ultra High Field Facility, for example, envisage to provide field intensities in excess of 10^{20} W/cm² and field frequencies in the x-ray domain [1–6]. Such facilities open the possibility of probing light-matter interaction in the ultra-relativistic regime [7–9]. In this regime, the quantum dynamical interaction of electrons, ions, or atoms can be modified due to relativistic corrections of the Dirac equation to the nonrelativistic Schrödinger equation. In certain setups, however, relativistic effects may change the dynamics not only quantitatively, but also qualitatively. As an example, spin-orbit interaction, that is, the interaction of a particle's spin with its orbital angular momentum, can lead to a splitting of atomic energy levels, which are degenerated within the framework of nonrelativistic quantum theory. At ultra-high laser intensities also, spin effects can set in [10–12].

In our recent publication [13], we demonstrated that relativistic effects may also modify the spin dynamics of an electron in external electromagnetic waves with elliptical polarization. This effect can be attributed to a coupling of the spin density that is associated with the external laser field to the electron's spin. The coupling between the electronic spin and the photonic spin is of similar origin as the well-known spin-orbit effect. Both effects have in common that two angular momentum degrees of freedom are coupled that are of different origin. Other examples for the interaction between different kinds of angular momentum have been studied in very different contexts, e. g., the angular momentum of phonons in a magnetic crystal and the angular momentum of the crystal [14] or the orbital angular momentum of light and the internal degrees of motion in molecules [15], to mention two recent examples.

In this contribution, we elaborate and extend the theoretical description of the electron's spin dynamics as studied in Ref. [13]. The article is organized as follows. In Sec. 2 we describe the considered laser setup and derive the electron's

quantum mechanical equations of motion, relativistic and non-relativistic. Subsequently, we solve these equations via time-dependent perturbation theory in Sec. 3 and by numerical methods in Sec. 4. In Sec. 5 we estimate under which experimental conditions the predicted spin precession may be realized before we summarize our results in Sec. 6.

2. Electrons in standing laser fields

2.1. Laser fields with elliptical polarization

We examine electrons in standing light waves formed by two counterpropagating laser beams with circular or elliptic polarization. The electric and magnetic field components of two elliptically polarized laser fields counterpropagating in the direction of the x axis are given by

$$\mathbf{E}_{1,2}(\mathbf{r}, t) = \hat{E} \left(\cos \frac{2\pi(x \mp ct)}{\lambda} \mathbf{e}_y + \cos \left(\frac{2\pi(x \mp ct)}{\lambda} \pm \eta \right) \mathbf{e}_z \right), \quad (1a)$$

$$\mathbf{B}_{1,2}(\mathbf{r}, t) = \frac{\hat{E}}{c} \left(\mp \cos \left(\frac{2\pi(x \mp ct)}{\lambda} \pm \eta \right) \mathbf{e}_y \pm \cos \frac{2\pi(x \mp ct)}{\lambda} \mathbf{e}_z \right). \quad (1b)$$

Here, we have introduced the speed of light c , the position vector $\mathbf{r} = (x, y, z)^T$, the time t , and \mathbf{e}_x , \mathbf{e}_y , and \mathbf{e}_z denoting unit vectors in the direction of the coordinate axes. The two electromagnetic waves (1) feature the same wavelength λ , the same electric field amplitude \hat{E} , and the same intensity

$$I = \varepsilon_0 c \hat{E}^2 \quad (2)$$

but have opposite helicity. The parameter $\eta \in (-\pi, \pi]$ determines the degree of ellipticity with $\eta = 0$ and $\eta = \pi$ corresponding to linear polarization and $\eta = \pm\pi/2$ to circular polarization. Introducing the wave number $k = 2\pi/\lambda$ and the lasers' angular frequency $\omega = kc$, the total electric and magnetic fields of the standing laser wave that is formed by superimposing the two

* heiko.bauke@mpi-hd.mpg.de

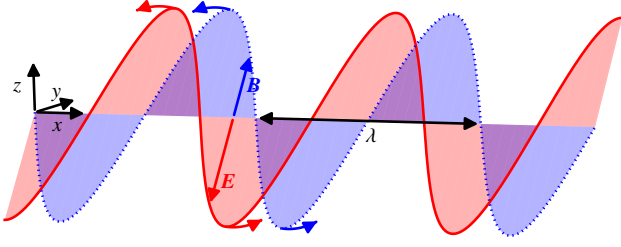


FIG. 1: (Color online) Schematic illustration of the electric (solid red line) and magnetic (dotted blue line) field components of the standing laser wave (3) with $\eta = \pi/2$ that is a superposition of two counter-propagating circularly polarized laser waves of opposite helicity and equal wavelength λ . The electric and magnetic components \mathbf{E} and \mathbf{B} are parallel to each other and rotate around the propagation direction.

electric and magnetic field components (1a) and (1b) follow as

$$\mathbf{E}(\mathbf{r}, t) = 2\hat{E} \cos kx (\cos \omega t \mathbf{e}_y + \cos(\omega t - \eta) \mathbf{e}_z), \quad (3a)$$

$$\mathbf{B}(\mathbf{r}, t) = \frac{2\hat{E}}{c} \sin kx (-\sin(\omega t - \eta) \mathbf{e}_y + \sin \omega t \mathbf{e}_z). \quad (3b)$$

For circular fields ($\eta = \pi/2$), the electric and the magnetic components (3) are parallel to each other and rotate around the propagation direction as sketched in Fig. 1.

The elliptically polarized fields (1) carry spin angular momentum [16, 17]. The partition of a general light beam's total angular momentum into orbital angular momentum and spin angular momentum was debated in the literature. A definition that seems to be well established now [18–21] utilizes Coulomb gauge vector potentials for both the magnetic as well as the electric field component. The Coulomb gauge vector potentials $\mathbf{A}_{1,2}$ and $\mathbf{C}_{1,2}$ of the elliptically polarized fields (1) are

$$\mathbf{C}_{1,2}(\mathbf{r}, t) = -\frac{\hat{E}}{\omega} (\pm \sin(kx \mp \omega t \pm \eta) \mathbf{e}_y - \sin(kx \mp \omega t) \mathbf{e}_z), \quad (4a)$$

$$\mathbf{A}_{1,2}(\mathbf{r}, t) = -\frac{\hat{E}}{\omega} (\mp \sin(kx \mp \omega t) \mathbf{e}_y \mp \sin(kx \mp \omega t \pm \eta) \mathbf{e}_z). \quad (4b)$$

These potentials are related to the electromagnetic fields via $\mathbf{E}_{1,2} = -\dot{\mathbf{A}}_{1,2} = -c\nabla \times \mathbf{C}_{1,2}$, $\mathbf{B}_{1,2} = \nabla \times \mathbf{A}_{1,2} = -\dot{\mathbf{C}}_{1,2}/c$ and the potentials comply with the Coulomb gauge as $\nabla \cdot \mathbf{A}_{1,2} = \nabla \cdot \mathbf{C}_{1,2} = 0$. With these quantities the spin density of each laser field is given by the expression $\varepsilon_0(\mathbf{E}_{1,2} \times \mathbf{A}_{1,2} + c\mathbf{B}_{1,2} \times \mathbf{C}_{1,2})/2$, which reduces in the case of the plane wave fields (1) to

$$\frac{\varepsilon_0}{2} (\mathbf{E}_{1,2} \times \mathbf{A}_{1,2} + c\mathbf{B}_{1,2} \times \mathbf{C}_{1,2}) = \varepsilon_0 \mathbf{E}_{1,2} \times \mathbf{A}_{1,2} = \frac{\varepsilon_0 \hat{E}^2 \lambda \sin \eta}{2\pi c} \mathbf{e}_x. \quad (5)$$

The total photonic spin density of the setup is

$$\frac{\varepsilon_0}{2} (\mathbf{E} \times \mathbf{A} + c\mathbf{B} \times \mathbf{C}) = \frac{\varepsilon_0 \hat{E}^2 \lambda \sin \eta}{\pi c} \mathbf{e}_x, \quad (6)$$

with $\mathbf{E} = \mathbf{E}_1 + \mathbf{E}_2$, $\mathbf{B} = \mathbf{B}_1 + \mathbf{B}_2$, $\mathbf{A} = \mathbf{A}_1 + \mathbf{A}_2$, and $\mathbf{C} = \mathbf{C}_1 + \mathbf{C}_2$. Thus, the ellipticity parameter η determines also the light's spin density.

Note, that for plane wave fields the photonic spin density may be expressed solely by the electric field and the magnetic vector potential, see (5), and many works utilize the expression $\varepsilon_0 \mathbf{E} \times \mathbf{A}$ to define the photonic spin density, which is not equivalent to $\varepsilon_0(\mathbf{E} \times \mathbf{A} + c\mathbf{B} \times \mathbf{C})/2$ for non-plane-wave fields, e. g., standing waves. The total amount of spin angular momentum, however, does not depend on which of both densities is chosen [22], this means

$$\int \varepsilon_0 \mathbf{E} \times \mathbf{A} d^3r = \int \frac{\varepsilon_0}{2} (\mathbf{E} \times \mathbf{A} + c\mathbf{B} \times \mathbf{C}) d^3r, \quad (7)$$

where the integration goes over all space regions with non-vanishing electromagnetic fields.

Furthermore, note that the given expressions for the photonic spin density require that the electromagnetic vector potentials \mathbf{A} and \mathbf{C} are given in Coulomb gauge. If another gauge is applied then \mathbf{A} and \mathbf{C} in the definition of the spin density have to be replaced by \mathbf{A}^\perp and \mathbf{C}^\perp , which are defined by splitting the vector potentials \mathbf{A} and \mathbf{C} such that $\mathbf{A} = \mathbf{A}^\perp + \mathbf{A}^\parallel$ and $\nabla \cdot \mathbf{A}^\perp = 0$ and $\nabla \times \mathbf{A}^\parallel = 0$ and similarly for the electric vector potential \mathbf{C} [23]. Thus the Coulomb gauge is the most convenient gauge to study effects of the photonic spin and it is therefore employed here. All predicted effects of this contribution result from gauge invariant quantum mechanical wave equations and are, therefore, independent of the choice of the gauge.

2.2. Quantum dynamics in momentum space

Introducing the window function, which allows for a smooth turn-on and turn-off of the laser field,

$$w(t) = \begin{cases} \sin^2 \frac{\pi t}{2\Delta T} & \text{if } 0 \leq t \leq \Delta T, \\ 1 & \text{if } \Delta T \leq t \leq T - \Delta T, \\ \sin^2 \frac{\pi(T-t)}{2\Delta T} & \text{if } T - \Delta T \leq t \leq T, \end{cases} \quad (8)$$

the magnetic vector potential of the combined laser fields (3) is given by

$$\mathbf{A}(\mathbf{r}, t) = -\frac{2w(t)\hat{E}}{\omega} \cos kx (\sin \omega t \mathbf{e}_y + \sin(\omega t - \eta) \mathbf{e}_z). \quad (9)$$

The parameters T and ΔT denote the total interaction time and the turn-on and turn-off intervals. The quantum mechanical evolution of an electron of mass m and charge $q = -e$ in the laser field with the vector potential (9) is governed by the Dirac equation

$$i\hbar \Psi(\mathbf{r}, t) = (c\boldsymbol{\alpha} \cdot (-i\hbar\nabla - q\mathbf{A}(\mathbf{r}, t)) + mc^2\beta) \Psi(\mathbf{r}, t) \quad (10)$$

with the Dirac matrices $\boldsymbol{\alpha} = (\alpha_x, \alpha_y, \alpha_z)^\top$ and β [24, 25]. The quasi one-dimensional sinusoidal structure of the vector potential (9) allows us to cast the partial differential equation (10) into a set of coupled ordinary differential equations [12]. For this purpose, we make the ansatz

$$\Psi(\mathbf{r}, t) = \sum_{n,\gamma} c_n^\gamma(t) \psi_n^\gamma(\mathbf{r}) \quad (11)$$

with integer n , $\gamma \in \{+\uparrow, -\uparrow, +\downarrow, -\downarrow\}$, and the four-component basis functions

$$\psi_n^\gamma(\mathbf{r}) = \sqrt{\frac{k}{2\pi}} u_n^\gamma e^{inkx}, \quad (12)$$

with u_n^γ defined as

$$u_n^{+\uparrow/\downarrow} = \sqrt{\frac{\mathcal{E}_n + mc^2}{2\mathcal{E}_n}} \begin{pmatrix} \chi^{\uparrow/\downarrow} \\ \frac{nck\hbar\sigma_x}{\mathcal{E}_n + mc^2} \chi^{\uparrow/\downarrow} \end{pmatrix}, \quad (13a)$$

$$u_n^{-\uparrow/\downarrow} = \sqrt{\frac{\mathcal{E}_n + mc^2}{2\mathcal{E}_n}} \begin{pmatrix} -\frac{nck\hbar\sigma_x}{\mathcal{E}_n + mc^2} \chi^{\uparrow/\downarrow} \\ \chi^{\uparrow/\downarrow} \end{pmatrix}, \quad (13b)$$

$\chi^\uparrow = (1, 0)^\top$, and $\chi^\downarrow = (0, 1)^\top$, and the relativistic energy-momentum relation

$$\mathcal{E}_n = \sqrt{(mc^2)^2 + (nck\hbar)^2}. \quad (14)$$

Introducing the four-tuples

$$c_n(t) = (c_n^{+\uparrow}(t), c_n^{+\downarrow}(t), c_n^{-\uparrow}(t), c_n^{-\downarrow}(t))^\top \quad (15)$$

and employing the expansion (11) the Dirac equation becomes in momentum space

$$i\hbar\dot{c}_n(t) = \mathcal{E}_n\beta c_n(t) + \sum_{n'} V_{n,n'}(t)c_{n'}(t). \quad (16)$$

Here, $V_{n,n'}(t)$ denotes the interaction Hamiltonian. Its components are given by

$$V_{n,n'}^{\gamma,\gamma'}(t) = \frac{w(t)q\hat{E}}{k} (\delta_{n,n'-1} + \delta_{n,n'+1}) \times \\ (u_n^{\gamma\dagger} \alpha_y u_{n'}^{\gamma'} \sin \omega t + u_n^{\gamma\dagger} \alpha_z u_{n'}^{\gamma'} \sin(\omega t - \eta)), \quad (17)$$

with $\gamma, \gamma' \in \{+\uparrow, -\uparrow, +\downarrow, -\downarrow\}$ and $\delta_{n,n'}$ denoting the Kronecker delta. As the basis functions (13) are common eigenfunctions of the free Dirac Hamiltonian, the canonical momentum operator, as well as of the z component of the Foldy-Wouthuysen spin operator [26], the spin expectation value (with the z axis as the quantization axis) is conveniently given by the absolute squared values of the coefficients $c_n^\gamma(t)$ via

$$s_z(t) = \frac{\hbar}{2} \sum_n (|c_n^{+\uparrow}(t)|^2 + |c_n^{-\uparrow}(t)|^2 - |c_n^{+\downarrow}(t)|^2 - |c_n^{-\downarrow}(t)|^2). \quad (18)$$

In order to interpret the electron's relativistic quantum dynamics it will be beneficial to consider the weakly relativistic limit of the Dirac equation (10). In this limit, this equation reduces via a Foldy-Wouthuysen transformation [26–28] to

$$i\hbar\dot{\Psi}(\mathbf{r}, t) = \left(\frac{(-i\hbar\nabla - q\mathbf{A}(\mathbf{r}, t))^2}{2m} - \frac{q\hbar}{2m} \boldsymbol{\sigma} \cdot \mathbf{B}(\mathbf{r}, t) + q\phi(\mathbf{r}, t) \right. \\ \left. - \frac{(-i\hbar\nabla - q\mathbf{A}(\mathbf{r}, t))^4}{8m^3c^2} - \frac{q^2\hbar^2}{8m^3c^4} (c^2\mathbf{B}(\mathbf{r}, t)^2 - \mathbf{E}(\mathbf{r}, t)^2) \right. \\ \left. - \frac{q\hbar}{4m^2c^2} \boldsymbol{\sigma} \cdot (\mathbf{E}(\mathbf{r}, t) \times (-i\hbar\nabla - q\mathbf{A}(\mathbf{r}, t))) - \frac{q\hbar^2}{8m^2c^2} \nabla \cdot \mathbf{E}(\mathbf{r}, t) \right. \\ \left. + \frac{q\hbar}{8m^3c^2} \left\{ \boldsymbol{\sigma} \cdot \mathbf{B}(\mathbf{r}, t), (-i\hbar\nabla - q\mathbf{A}(\mathbf{r}, t))^2 \right\} \right) \Psi(\mathbf{r}, t) \quad (19)$$

for the now two-component wave function $\Psi(\mathbf{r}, t)$ with $\mathbf{A}(\mathbf{r}, t)$ given by (9), $\mathbf{B}(\mathbf{r}, t) = \nabla \times \mathbf{A}(\mathbf{r}, t)$, $\mathbf{E}(\mathbf{r}, t) = -\dot{\mathbf{A}}(\mathbf{r}, t)$, and the vector of Pauli matrices $\boldsymbol{\sigma} = (\sigma_x, \sigma_y, \sigma_z)^\top$. In leading order Eq. (19) features four terms that may cause spin dynamics. The so-called Zeeman term $\sim \boldsymbol{\sigma} \cdot \mathbf{B}(\mathbf{r}, t)$ mediates the coupling of the electron's spin to the magnetic field and the anticommutator expression $\sim \{\boldsymbol{\sigma} \cdot \mathbf{B}(\mathbf{r}, t), (-i\hbar\nabla - q\mathbf{A}(\mathbf{r}, t))^2\}$ is the lowest order relativistic correction to the Zeeman coupling. It is well-known that the term $\sim \boldsymbol{\sigma} \cdot \mathbf{E}(\mathbf{r}, t) \times i\hbar\nabla$ in (19) leads to the so-called spin-orbit interaction, i. e., the coupling between the electron's spin and its orbital angular momentum. The term $\sim \boldsymbol{\sigma} \cdot (\mathbf{E}(\mathbf{r}, t) \times \mathbf{A}(\mathbf{r}, t))$, however, may be interpreted as a coupling of the spin density of the external electromagnetic wave to the particle's spin. In Sec. 4 we will show that the relativistic electron motion in the setup of Sec. 2 can be described in leading order by the nonrelativistic Pauli equation complemented by the relativistic correction due to the electromagnetic wave's spin density as the only relativistic correction. This leads us to the relativistic Pauli equation

$$i\hbar\dot{\Psi}(\mathbf{r}, t) = \left(\frac{1}{2m} (-i\hbar\nabla - q\mathbf{A}(\mathbf{r}, t))^2 - \frac{q\hbar}{2m} \boldsymbol{\sigma} \cdot \mathbf{B}(\mathbf{r}, t) \right. \\ \left. + \frac{q^2\hbar}{4m^2c^2} \boldsymbol{\sigma} \cdot (\mathbf{E}(\mathbf{r}, t) \times \mathbf{A}(\mathbf{r}, t)) \right) \Psi(\mathbf{r}, t). \quad (20)$$

We also formulate the relativistic Pauli equation (20) in momentum space by utilizing the ansatz (11) as for the Dirac equation but now with $\gamma \in \{\uparrow, \downarrow\}$ and the two-component basis functions

$$\psi_n^\gamma(\mathbf{r}) = \sqrt{\frac{k}{2\pi}} \chi^\gamma e^{inkx}. \quad (21)$$

Using the expansion (11) with the functions (21) and introducing the pair

$$c_n(t) = (c_n^\uparrow(t), c_n^\downarrow(t))^\top, \quad (22)$$

the relativistic Pauli (20) is given in momentum space by

$$i\hbar\dot{c}_n(t) = \frac{n^2k^2\hbar^2}{2m} c_n(t) \\ + \frac{q^2\hat{E}^2w(t)^2}{2k^2mc^2} (1 - \cos \eta \cos(2\omega t - \eta))(c_{n-2}(t) + 2c_n(t) + c_{n+2}(t)) \\ + \frac{i\hbar q\hat{E}w(t)}{2mc} (-\sigma_y \sin(\omega t - \eta) + \sigma_z \sin \omega t)(c_{n-1}(t) - c_{n+1}(t)) \\ + \frac{\hbar q^2\hat{E}^2w(t)^2 \sin \eta}{4km^2c^3} \sigma_x (c_{n-2}(t) + 2c_n(t) + c_{n+2}(t)). \quad (23)$$

Neglecting also the relativistic corrections due to the term $\sim \boldsymbol{\sigma} \cdot (\mathbf{E}(\mathbf{r}, t) \times \mathbf{A}(\mathbf{r}, t))$ in (20), Eq. (23) reduces to the nonrelativistic Pauli equation in momentum space

$$i\hbar\dot{c}_n(t) = \frac{n^2k^2\hbar^2}{2m} c_n(t) \\ + \frac{q^2\hat{E}^2w(t)^2}{2k^2mc^2} (1 - \cos \eta \cos(2\omega t - \eta))(c_{n-2}(t) + 2c_n(t) + c_{n+2}(t)) \\ + \frac{i\hbar q\hat{E}w(t)}{2mc} (-\sigma_y \sin(\omega t - \eta) + \sigma_z \sin \omega t)(c_{n-1}(t) - c_{n+1}(t)). \quad (24)$$

The two-component basis functions (21) are common eigenfunctions of the free Pauli Hamiltonian, the canonical momentum operator, and the nonrelativistic spin operator $\hbar\sigma_z/2$. Thus, the spin expectation value (with the z axis as the quantization axis) is given by the absolute squared values of the coefficients $c_n^\gamma(t)$ via

$$s_z(t) = \frac{\hbar}{2} \sum_n |c_n^\uparrow(t)|^2 - |c_n^\downarrow(t)|^2. \quad (25)$$

Equations (16), (23), and (24) are the basic equations that we are going to solve in the next sections numerically and analytically via time-dependent perturbation theory. In the following, we assume that the electron is initially at rest with spin aligned to the z axis, which corresponds to the initial condition $c_0^{\uparrow\uparrow}(0) = 1$ (or $c_0^\uparrow(0) = 1$ in case of the Pauli equation) and $c_n^\gamma(0) = 0$ else.

3. Time-dependent perturbation theory

The short-time evolution of the electron dynamics may be calculated via time-dependent perturbation theory [29] that allows us to devise an analytic expression for the Rabi frequency of the spin precession. In this scheme the Hamiltonian is split into a free part and a possibly time-dependent interaction part, viz., $H = H_0 + V(t)$. Then the time evolution operator that maps a quantum state from time 0 to time t is given by

$$U(t) = U_0(t) + U_1(t) + U_2(t) + \dots \quad (26)$$

with the free propagator

$$U_0(t) = \exp\left(-\frac{i}{\hbar}H_0t\right) \quad (27)$$

and the corrections due to the interaction Hamiltonian $V(t)$

$$U_n(t) = \frac{1}{(i\hbar)^n} \int_0^t dt_n \dots \int_0^{t_3} dt_2 \int_0^{t_2} dt_1 U_0(t-t_n)V(t_n) \dots U_0(t_2-t_1)V(t_1)U_0(t_1) \quad (28)$$

for $n > 0$. To simplify the following calculations we neglect the turn-on and turn-off times; i. e., we set $\Delta T = 0$ for the remainder of this section. Furthermore, we specialize to the case of laser waves with circular polarization, i. e., $\eta = \pi/2$.

3.1. Dirac equation

For the Dirac equation in momentum space (16) the operators H_0 , $V(t)$, and $U_0(t, 0)$ are represented by matrices of infinite dimension that we will conveniently write in terms of submatrices of size 2×2 and 4×4 . First, we introduce the 2×2

matrices

$$V_{y;n,n'}^{\zeta,\zeta'} = \begin{pmatrix} u_n^{\zeta,\uparrow\uparrow} \alpha_y u_{n'}^{\zeta',\uparrow} & u_n^{\zeta,\uparrow\downarrow} \alpha_y u_{n'}^{\zeta',\downarrow} \\ u_n^{\zeta,\downarrow\uparrow} \alpha_y u_{n'}^{\zeta',\uparrow} & u_n^{\zeta,\downarrow\downarrow} \alpha_y u_{n'}^{\zeta',\downarrow} \end{pmatrix}, \quad (29a)$$

$$V_{z;n,n'}^{\zeta,\zeta'} = \begin{pmatrix} u_n^{\zeta,\uparrow\uparrow} \alpha_z u_{n'}^{\zeta',\uparrow} & u_n^{\zeta,\uparrow\downarrow} \alpha_z u_{n'}^{\zeta',\downarrow} \\ u_n^{\zeta,\downarrow\uparrow} \alpha_z u_{n'}^{\zeta',\uparrow} & u_n^{\zeta,\downarrow\downarrow} \alpha_z u_{n'}^{\zeta',\downarrow} \end{pmatrix}, \quad (29b)$$

and

$$V_{n,n'}^{\zeta,\zeta'}(t) = \frac{q\hat{E}}{k} (\delta_{n,n'-1} + \delta_{n,n'+1}) \times (V_{y;n,n'}^{\zeta,\zeta'} \sin \omega t - V_{z;n,n'}^{\zeta,\zeta'} \cos \omega t), \quad (29c)$$

with $\zeta, \zeta' \in \{+, -\}$. We further introduce the 4×4 matrix

$$V_{n,n'}(t) = \begin{pmatrix} V_{n,n'}^{++}(t) & V_{n,n'}^{+-}(t) \\ V_{n,n'}^{-+}(t) & V_{n,n'}^{--}(t) \end{pmatrix} \quad (30)$$

that comprises 16 matrix elements (17) of the interaction Hamiltonian $V(t)$. In this notation, the free Hamiltonian H_0 reads

$$H_{0;n,n'} = \begin{pmatrix} \mathcal{E}_n \mathbb{1} & 0 \\ 0 & -\mathcal{E}_n \mathbb{1} \end{pmatrix} \delta_{n,n'}. \quad (31)$$

Consequently, matrix elements of the free propagator (27) are given by

$$U_{0;n,n'}(t) = \begin{pmatrix} U_{0;n,n'}^{++}(t) & 0 \\ 0 & U_{0;n,n'}^{--}(t) \end{pmatrix} \quad (32)$$

with

$$U_{0;n,n'}^{++}(t) = \exp(-i\mathcal{E}_n t/\hbar) \delta_{n,n'} \mathbb{1}, \quad (33a)$$

$$U_{0;n,n'}^{--}(t) = \exp(i\mathcal{E}_n t/\hbar) \delta_{n,n'} \mathbb{1}. \quad (33b)$$

As our numerical simulations indicate that spin changing quantum transitions occur from the state with coefficient $c_0^{\uparrow\uparrow}$ to the state with $c_0^{\downarrow\downarrow}$, we do not need to calculate the full time evolution matrix, knowing

$$U_{0,0}^{++}(t) = U_{0;0,0}^{++}(t) + U_{1;0,0}^{++}(t) + U_{2;0,0}^{++}(t) + U_{3;0,0}^{++}(t) + U_{4;0,0}^{++}(t) + \dots \quad (34)$$

will be sufficient. A short calculation shows that $U_{n;0,0}^{++}(t)$ is a zero matrix for odd n . In the following we will calculate the propagators in second and fourth order time-dependent perturbation theory.

First, we calculate the second-order propagator, that is, according to (28),

$$U_{2;0,0}^{++}(t) = -\frac{1}{\hbar^2} \int_0^t dt_2 \int_0^{t_2} dt_1 U_{0;0,0}^{++}(t-t_2) (V_{0,1}^{++}(t_2) U_{0;1,1}^{++}(t_2-t_1) V_{1,0}^{++}(t_1) + V_{0,1}^{+-}(t_2) U_{0;1,1}^{--}(t_2-t_1) V_{1,0}^{+-}(t_1) + V_{0,-1}^{++}(t_2) U_{0;-1,-1}^{++}(t_2-t_1) V_{-1,0}^{++}(t_1) + V_{0,-1}^{+-}(t_2) U_{0;-1,-1}^{--}(t_2-t_1) V_{-1,0}^{+-}(t_1)) U_{0;0,0}^{++}(t_1). \quad (35)$$

Note that in the last equation we took advantage of the fact that the interaction Hamiltonian and the free particle propagator are banded matrices. Rewriting the matrix elements (29c) of the interaction Hamiltonian by expanding the trigonometric functions into exponentials

$$V_{n,n'}^{\zeta,\zeta'}(t) = \frac{q\hat{E}}{2k} (\delta_{n,n'-1} + \delta_{n,n'+1}) \times \\ \left((-iV_{y,n,n'}^{\zeta,\zeta'} - V_{z,n,n'}^{\zeta,\zeta'}) e^{i\omega t} + (iV_{y,n,n'}^{\zeta,\zeta'} - V_{z,n,n'}^{\zeta,\zeta'}) e^{-i\omega t} \right), \quad (36)$$

and utilizing the identity

$$\begin{pmatrix} \pm iV_{y,n,n'}^{++} - V_{z,n,n'}^{++} & \pm iV_{y,n,n'}^{+-} - V_{z,n,n'}^{+-} \\ \pm iV_{y,n,n'}^{-+} - V_{z,n,n'}^{-+} & \pm iV_{y,n,n'}^{--} - V_{z,n,n'}^{--} \end{pmatrix} = \\ \begin{pmatrix} r_{n,n'}(\mp\sigma_z + i\sigma_y) & t_{n,n'}(\pm i\sigma_y - \sigma_z) \\ t_{n,n'}(\pm i\sigma_y - \sigma_z) & r_{n,n'}(\pm\sigma_z - i\sigma_y) \end{pmatrix} \quad (37)$$

with the coefficients

$$t_{n,n'} = d_n^+ d_{n'}^+ + d_n^- d_{n'}^-, \quad (38)$$

$$r_{n,n'} = d_n^- d_{n'}^+ - d_n^+ d_{n'}^-, \quad (39)$$

and

$$d_n^+ = \frac{1}{\sqrt{2}} \sqrt{1 + \frac{mc^2}{\mathcal{E}_n}}, \quad (40a)$$

$$d_n^- = \frac{\text{sgn } n}{\sqrt{2}} \sqrt{1 - \frac{mc^2}{\mathcal{E}_n}} \quad (40b)$$

the integral (35) evaluates to [30]

$$U_{2;0,0}^{++}(t) = i \frac{q^2 \hat{E}^2}{2k^2} e^{-i\mathcal{E}_0 t/\hbar} t \times \\ \left(\frac{r_{0,1} r_{1,0} (-\mathbb{1} + \sigma_x)}{-\mathcal{E}_1 + \mathcal{E}_0 - \hbar\omega} + \frac{r_{0,1} r_{1,0} (-\mathbb{1} - \sigma_x)}{-\mathcal{E}_1 + \mathcal{E}_0 + \hbar\omega} + \frac{r_{0,-1} r_{-1,0} (-\mathbb{1} + \sigma_x)}{-\mathcal{E}_{-1} + \mathcal{E}_0 - \hbar\omega} \right. \\ \left. + \frac{r_{0,-1} r_{-1,0} (-\mathbb{1} - \sigma_x)}{-\mathcal{E}_{-1} + \mathcal{E}_0 + \hbar\omega} + \frac{t_{0,1} t_{1,0} (\mathbb{1} - \sigma_x)}{\mathcal{E}_1 + \mathcal{E}_0 - \hbar\omega} + \frac{t_{0,1} t_{1,0} (\mathbb{1} + \sigma_x)}{\mathcal{E}_1 + \mathcal{E}_0 + \hbar\omega} \right. \\ \left. + \frac{t_{0,-1} t_{-1,0} (\mathbb{1} - \sigma_x)}{\mathcal{E}_{-1} + \mathcal{E}_0 - \hbar\omega} + \frac{t_{0,-1} t_{-1,0} (\mathbb{1} + \sigma_x)}{\mathcal{E}_{-1} + \mathcal{E}_0 + \hbar\omega} \right) + O(1). \quad (41)$$

Note, that we give in (41) only those terms explicitly that grow linear in time t . Terms that oscillate but remain bounded over time are omitted. Summing the various terms in (41) finally yields

$$U_{2;0,0}^{++}(t) = -i \frac{q^2 \hat{E}^2}{2k^2 mc^2} e^{-i\mathcal{E}_0 t/\hbar} t. \quad (42)$$

Thus, $U_{2;0,0}^{++}(t)$ is diagonal and therefore no spin flip is predicted in second order time-dependent perturbation theory.

The fourth order time-dependent perturbation theory propagator is explicitly given by

$$U_{4;0,0}^{++}(t) = \frac{1}{\hbar^4} \int_0^t dt_4 \int_0^{t_4} dt_3 \int_0^{t_3} dt_2 \int_0^{t_2} dt_1 \\ \sum_{(n_1, n_2, n_3)} \sum_{\substack{\zeta_1, \zeta_2, \zeta_3 \\ \in \{+, -\}}} U_{0;0,0}^{++}(t-t_4) V_{0,n_3}^{+\zeta_3}(t_4) U_{0;n_3, n_3}^{\zeta_3, \zeta_3}(t_4-t_3) V_{n_3, n_2}^{\zeta_3, \zeta_2}(t_3) U_{0;n_2, n_2}^{\zeta_2, \zeta_2}(t_3-t_2) V_{n_2, n_1}^{\zeta_2, \zeta_1}(t_2) U_{0;n_1, n_1}^{\zeta_1, \zeta_1}(t_2-t_1) V_{n_1, 0}^{\zeta_1, +}(t_1) U_{0;0,0}^{++}(t_1), \quad (43)$$

where the multi-indices (n_1, n_2, n_3) and $(\zeta_1, \zeta_2, \zeta_3)$ can take six and eight different values, respectively. Thus the sum in (43) runs over 48 terms. All possible values of the tuple (n_1, n_2, n_3) are shown in Tab. 1. Expanding the trigonometric functions of the interaction Hamiltonian into exponentials and reordering the terms of (43) we get

$$U_{4;0,0}^{++}(t) = \\ \left(\frac{q\hat{E}}{2k\hbar} \right)^4 \sum_{(n_1, n_2, n_3)} \sum_{\substack{\zeta_1, \zeta_2, \zeta_3 \\ \in \{+, -\}}} \sum_{\substack{\eta_1, \eta_2, \eta_3, \eta_4 \\ \in \{+1, -1\}}} (-\eta_4 i V_{y,0,n_3}^{+\zeta_3} - V_{z,0,n_3}^{+\zeta_3}) (-\eta_3 i V_{y,n_3,n_2}^{\zeta_3, \zeta_2} - V_{z,n_3,n_2}^{\zeta_3, \zeta_2}) (-\eta_2 i V_{y,n_2,n_1}^{\zeta_2, \zeta_1} - V_{z,n_2,n_1}^{\zeta_2, \zeta_1}) (-\eta_1 i V_{y,n_1,0}^{\zeta_1, 0} - V_{z,n_1,0}^{\zeta_1, +}) \nu(t) \quad (44)$$

with the phase integral

$$\nu(t) = \int_0^t dt_4 \int_0^{t_4} dt_3 \int_0^{t_3} dt_2 \int_0^{t_2} dt_1 \\ \exp\left(-\frac{i}{\hbar} (\mathcal{E}_0(t-t_4) + \zeta_3 \mathcal{E}_{n_3}(t_4-t_3) + \zeta_2 \mathcal{E}_{n_2}(t_3-t_2) + \zeta_1 \mathcal{E}_{n_1}(t_2-t_1) + \mathcal{E}_0 t_1)\right) \exp(i\omega(\eta_4 t_4 + \eta_3 t_3 + \eta_2 t_2 + \eta_1 t_1)). \quad (45)$$

For those terms where the indices $\eta_1, \eta_2, \eta_3, \eta_4$ sum to zero the

phase integral grows linearly in time, viz.

TABLE 1: All six possible values of the multi-indices (n_1, n_2, n_3) that appear in the sums of (43) and (44) and in the integral (45).

number	n_1	n_2	n_3
1	1	2	1
2	1	0	1
3	1	0	-1
4	-1	-2	-1
5	-1	0	-1
6	-1	0	1

$$\nu(t) = \frac{i}{(\mathcal{E}_0 - \zeta_1 \mathcal{E}_{n_1})/\hbar - \eta_1 \omega} \frac{i}{(\mathcal{E}_0 - \zeta_2 \mathcal{E}_{n_2})/\hbar - (\eta_1 + \eta_2)\omega} \times \frac{i}{(\mathcal{E}_0 - \zeta_3 \mathcal{E}_{n_3})/\hbar - (\eta_1 + \eta_2 + \eta_3)\omega} e^{-i\mathcal{E}_0 t/\hbar} + O(1), \quad (46)$$

where $O(1)$ indicates some integration constant. If $\eta_1 + \eta_2 + \eta_3 + \eta_4 \neq 0$, the function $\nu(t)$ shows oscillatory behavior, and, therefore, these cases can be neglected.

A Taylor expansion of the propagator (44) up to the fourth order in the laser's wave number k yields finally

$$U_{4;0,0}^{++}(t) = i \left(\Omega_\varphi \mathbb{1} + \frac{\Omega}{2} \sigma_x \right) e^{-i\mathcal{E}_0 t/\hbar} + O(k^4), \quad (47)$$

with the two angular frequencies

$$\Omega_\varphi = \frac{q^4 \hat{E}^4 \lambda^6}{(2\pi)^6 \hbar^3 m c^4} \quad (48)$$

and

$$\Omega = \frac{q^4 \hat{E}^4 \lambda^5}{(2\pi)^5 \hbar^2 m^2 c^5}. \quad (49)$$

In contrast to the second order perturbation theory we have found now a contribution in the propagator that causes a spin precession around the x axis due to the σ_x term in (47). The fourth order short-time propagator yields for the initial condition $c_0^{+\uparrow}(0) = 1$ and $c_n^\gamma(0) = 0$ else the spin-flip probability

$$|c_0^{+\uparrow}(t)|^2 = \frac{\Omega^2 t^2}{4}. \quad (50)$$

Anticipating the oscillatory behavior of the long-time spin dynamics (see Sec. 4 and Ref. [13]), which means

$$|c_0^{+\uparrow}(t)|^2 = \sin^2 \frac{\Omega t}{2}, \quad (51)$$

we identify the frequency Ω as the precession frequency (49) of the electron's spin [12] by comparing the Taylor expansion of (51) with (50). The spin precession frequency (49) is proportional to the photonic spin density $\varrho_\sigma = \varepsilon_0 \hat{E}^2 \lambda / (\pi c)$, the laser field's intensity I given in (2), and the fourth power of the wavelength

$$\Omega = \varrho_\sigma I \lambda^4 \frac{\alpha_{\text{el}}^2}{2\pi^2 m^2 c^3}, \quad (52)$$

where the proportionality factor $\alpha_{\text{el}}^2 / (2\pi^2 m^2 c^3)$ is independent of the laser's electromagnetic field and α_{el} denotes the fine-structure constant.

3.2. Nonrelativistic Pauli equation

In order to calculate the precession frequency in the framework of the nonrelativistic Pauli equation (24) we define the "free" Hamiltonian

$$H_{0;n,n'} = \left(\frac{n^2 k^2 \hbar^2}{2m} + \frac{q^2 \hat{E}^2}{k^2 m c^2} \right) \delta_{n,n'} \mathbb{1}. \quad (53)$$

Then the interaction Hamiltonian becomes

$$V_{n,n'}(t) = V_{1;n,n'}(t) + V_{2;n,n'}(t) \quad (54a)$$

with

$$V_{1;n,n'}(t) = \frac{i\hbar q \hat{E}}{2mc} (\sigma_y \cos \omega t - \sigma_z \sin \omega t) (\delta_{n,n'+1} - \delta_{n,n'-1}), \quad (54b)$$

$$V_{2;n,n'}(t) = \frac{q^2 \hat{E}^2}{2k^2 m c^2} (\delta_{n,n'-2} + \delta_{n,n'+2}) \mathbb{1}. \quad (54c)$$

Neglecting the constant term $q^2 \hat{E}^2 / (k^2 m c^2)$ in (53), which causes just a global phase rotation that may be removed by a suitable gauge, yields the free propagator

$$U_{0;n,n'}(t) = \exp\left(-i \frac{n^2 k^2 \hbar}{2m} t\right) \delta_{n,n'} \mathbb{1}. \quad (55)$$

The second order propagator for the coefficient $c_0(t)$

$$U_{2;0,0}(t) = -\frac{1}{\hbar^2} \int_0^t dt_2 \int_0^{t_2} dt_1 U_{0;0,0}(t-t_2) \left(V_{2;0,2}(t_2) U_{0;2,2}(t_2-t_1) V_{2;2,0}(t_1) + V_{2;0,-2}(t_2) U_{0;-2,-2}(t_2-t_1) V_{2;-2,0}(t_1) + V_{1;0,1}(t_2) U_{0;1,1}(t_2-t_1) V_{1;1,0}(t_1) + V_{1;0,-1}(t_2) U_{0;-1,-1}(t_2-t_1) V_{1;-1,0}(t_1) \right) U_{0;0,0}(t_1) \quad (56)$$

becomes after time integration

$$U_{2;0,0}(t) = -i \frac{q^2 \hat{E}^2}{2m^2 c^2} \frac{k^2 \hbar^2 / (2m) \mathbb{1} + \omega \hbar \sigma_x}{(k^2 \hbar^2 / (2m))^2 - (\omega \hbar)^2} t + O(\hat{E}^4), \quad (57)$$

which reduces in the limit $k < m\hat{c}\hbar$ to

$$U_{2;0,0}(t) = i \left(\frac{\Omega_P \hbar k}{4mc} \mathbb{1} + \frac{\Omega_P}{2} \sigma_x \right) t, \quad (58)$$

where

$$\Omega_P = \frac{q^2 \hat{E}^2 \lambda}{2\pi m^2 c^3} \quad (59)$$

denotes the spin-precession angular frequency for the nonrelativistic Pauli equation. Note that in the case of the nonrelativistic Pauli equation already second order time-dependent perturbation theory predicts spin precession in contrast to the fully relativistic Dirac equation. Furthermore, spin-precession angular frequencies for the nonrelativistic Pauli equation (59) and the Dirac equation (49) feature qualitatively different dependencies on the electric field strength \hat{E} : quadratic scaling in the former case, quartic scaling in the latter case.

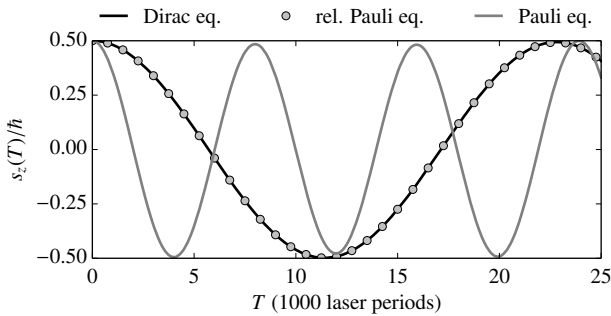


FIG. 2: Expectation value of the quantum mechanical electron spin in z direction $s_z(T)$ as a function of the total interaction time T by using three different equations of motion (the Dirac equation (16), the relativistic Pauli equation (23), and the nonrelativistic Pauli equation (24)) to model the quantum dynamics. The wavelength and the amplitude of the applied circularly polarized laser fields are $\lambda = 0.159$ nm and $\hat{E} = 2.057 \times 10^{14}$ V/m, respectively, and the field's switch-on-off interval ΔT corresponds to five laser cycles.

4. Numerical results

In order to corroborate our analytical results of Sec. 3, we carried out some numerical simulations solving the time-dependent Dirac equation as well as the time-dependent relativistic and nonrelativistic Pauli equations. Figure 2 shows the expectation value of the quantum mechanical electron spin in z direction $s_z(T)$ as a function of the total interaction time T . Time-dependent perturbation theory predicts different precession frequencies (49) and (59) for the nonrelativistic Pauli equation and for the Dirac equation, respectively. This is consistent with our numerical simulations, which yield oscillatory behavior of the spin with different angular frequencies for the nonrelativistic Pauli equation and for the Dirac equation; see Fig. 2. Note that the relativistic Pauli equation (23) and the Dirac equation (16) yield spin evolutions that are virtually indistinguishable. Thus, the relativistic Pauli equation is an excellent approximation to the fully relativistic Dirac equation for the setup and the parameters that we consider here.

In Fig. 3 we compare the angular frequencies of the spin precession that result from the nonrelativistic Pauli equation, the relativistic Pauli equation, and the fully relativistic Dirac equation for the case of circular polarization ($\eta = \pi/2$). Our numerical results reflect the different scaling of the angular frequency as a function of the peak electric field strength for the nonrelativistic Pauli equation and the Dirac equation. The numerical results for the spin-precession frequency are in an excellent agreement with the theoretical predictions (49) and (59), respectively. Note that the spin-precession frequency (49) for the Dirac equation also describes the spin-precession frequency that results from the relativistic Pauli equation very well. As demonstrated in Ref. [13] the spin precession angular frequency becomes proportional to $\sin \eta$ if the light has elliptical polarization. This means that the spin precession effect ceases to exist in the case of linear polarization ($\eta = 0$).

In Sec. 3.1 we demonstrated that in second order time-

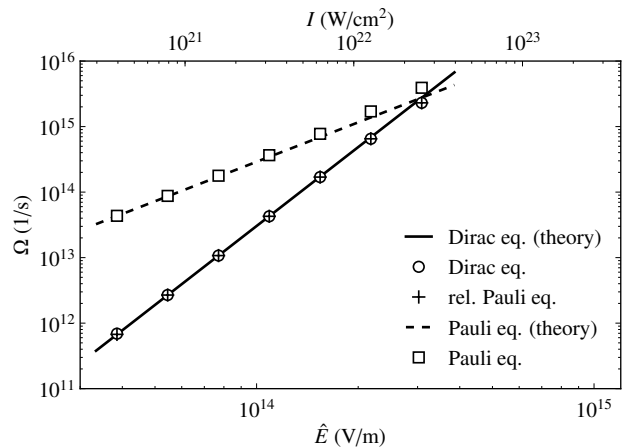


FIG. 3: Angular frequency Ω of the spin precession as a function of the laser's electric field strength \hat{E} and its intensity I for lasers of the wavelength $\lambda = 0.159$ nm. Depending on the applied theory (the Dirac equation (10), the relativistic Pauli equation (20), or the nonrelativistic Pauli equation) the spin of an electron in two counterpropagating circularly polarized light waves scales with the second or the fourth power of \hat{E} . Theoretical predictions for the spin-precession frequency are given by (49) and (59), respectively.

dependent perturbation theory for the Dirac equation there is no spin precession. In order to derive the spin-precession frequency we had to calculate the dynamics in fourth order perturbation theory. In second order perturbation theory for the relativistic Pauli theory the spin forces due to the magnetic field and the spin forces due to the light's spin density just cancel each other. As shown in Ref. [13], the cancellation of the spin forces can also be understood by quasi-classical considerations if one assumes that the electron is evenly spread over the range of a wavelength. The observed spin precession results because the electron's wave function actually accumulates at the maxima of the magnetic field of the standing light wave at $x = \pm\lambda/4$. In order to demonstrate this effect let us utilize the relativistic Pauli equation (20). A snapshot of the electron density $\varrho(x, t) = |\Psi_{\uparrow}(x, t)|^2 + |\Psi_{\downarrow}(x, t)|^2$ during the electron's interaction with the laser field is shown in the left part of Fig. 4; here Ψ_{\uparrow} and Ψ_{\downarrow} denote the upper and lower components of the wave function Ψ . The shape of the wave function can be characterized by calculating the density at $x = \lambda/4$. If the density $\varrho(x, t)$ is evenly distributed, then $\lambda\varrho(\lambda/4, t) = 1$. Thus, larger values indicate deviations from a flat distribution. As shown in the right part of Fig. 4, the electron density at $x = \lambda/4$ oscillates at frequencies much larger than the spin-precession frequency. The quantity $\lambda\varrho(\lambda/4, t)$ oscillates around some mean value that is larger than one and that depends on the electric field amplitude \hat{E} . Our numerical simulations indicate that the larger \hat{E} the more the electron density tends to concentrate around $x = \pm\lambda/4$. Furthermore, the wave packet shows a beating behavior as displayed in the right most part of Fig. 4. Note that the beat's envelope does not have the same period as the spin precession. Thus, the electron's spatial density and its spin oscillate in an asynchronous manner.

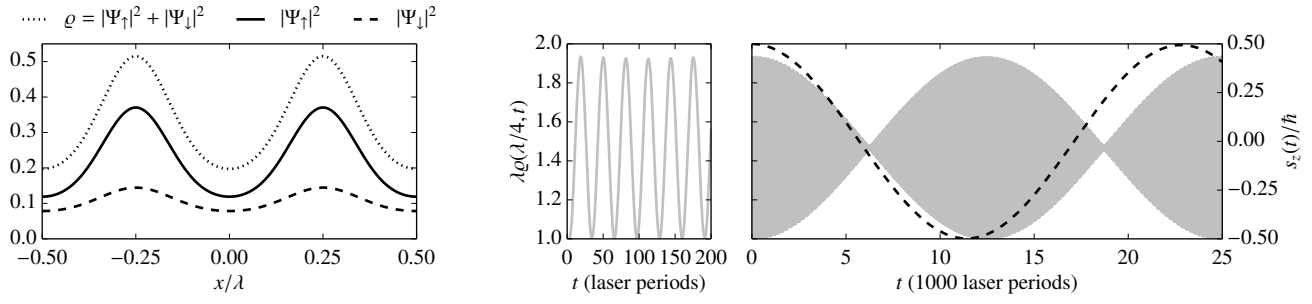


FIG. 4: Left display: Electron density $\rho = |\Psi_\uparrow|^2 + |\Psi_\downarrow|^2$ and densities of the individual spinor components $|\Psi_\uparrow|^2$ and $|\Psi_\downarrow|^2$, respectively, after $t = 4400$ laser periods. The densities accumulate in regions of high magnetic fields near $x = \pm\lambda/4$. Right displays: The scaled electron density $\lambda\rho(x, t)$ at $x = \lambda/4$ (solid gray line, left axis) and the expectation value of the spin $s_z(t)$ (dashed black line, right axis) as a function of time t . All laser parameters as in Fig. 2. Note that oscillations of $\rho(\lambda/4, t)$ are too fast to be resolved on the scale of the right most display.

5. Considerations on the electric field strength

The sinusoidal oscillatory motion of the electron's spin in the standing laser field of two elliptically polarized laser fields is of perturbative character. It starts to breakdown if the laser field becomes too strong resulting in an anharmonic motion of the spin. Criteria for the breakdown of the harmonic spin precession may be devised from the relativistic Pauli equation (23). The external laser field can be treated as a small perturbation if the kinetic-energy coefficient $k^2\hbar^2/(2m)$ in (23) is large compared to the others. This means the conditions

$$\frac{q^2\hat{E}^2}{2k^2mc^2} < \frac{k^2\hbar^2}{2m}, \quad \frac{\hbar|q|\hat{E}}{2mc^2} < \frac{k^2\hbar^2}{2m}, \quad \frac{\hbar q^2\hat{E}^2}{4km^2c^3} < \frac{k^2\hbar^2}{2m} \quad (60)$$

have to be met. The first two inequalities are both equivalent to

$$\frac{|q|\hat{E}}{k^2\hbar c} < 1 \quad (61a)$$

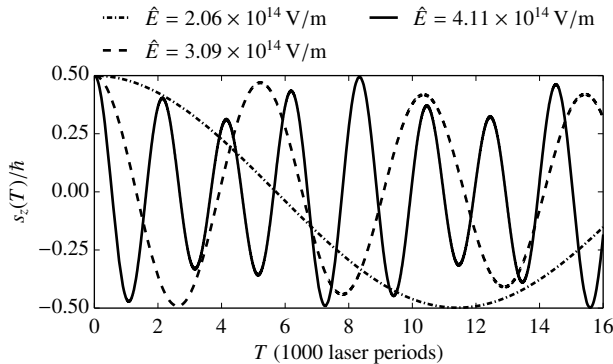


FIG. 5: Expectation value of the quantum mechanical electron spin in z direction $s_z(T)$ as a function of the total interaction time T for different peak electric field strengths \hat{E} . Other parameters as in Fig. 2. The quantum dynamics was simulated by solving the time-dependent Dirac equation.

and from the third inequality of (60) follows with (61a)

$$\frac{|q|\hat{E}}{2kmc^2} < 1. \quad (61b)$$

For laser wavelengths that are longer than half of the Compton wavelength the condition (61b) is always fulfilled provided that the condition (61a) is met. In Fig. 5 we show the spin dynamics for three different peak electric field strengths, for the cases $|q|\hat{E}/(k^2\hbar c) < 1$ with $\hat{E} = 2.06 \times 10^{14}$ V/m, $|q|\hat{E}/(k^2\hbar c) \approx 1$ with $\hat{E} = 3.09 \times 10^{14}$ V/m, and $|q|\hat{E}/(k^2\hbar c) > 1$ with $\hat{E} = 4.11 \times 10^{14}$ V/m, respectively. The figure clearly shows how the inharmonicities start to set in at $|q|\hat{E}/(k^2\hbar c) \approx 1$.

Generally speaking the observed electron-spin dynamics is not a strong-field effect. Spin flips may be observed also for weak laser fields but the spin-precession frequency becomes small in this regime. In this case, the electron must be trapped for many laser cycles in the laser field's focus to observe a full spin flip. If one assumes that the electron stays for \mathcal{N} cycles in the laser's focus, then the required electric field strength is bounded as

$$\left(\frac{\omega^6\hbar^2m^2}{2Nq^4}\right)^{1/4} = \left(\frac{(2\pi)^6c^6\hbar^2m^2}{2Nq^4\lambda^6}\right)^{1/4} < \hat{E} < \frac{\omega^2\hbar}{|q|c} = \frac{(2\pi)^2c\hbar}{|q|\lambda^2}. \quad (62)$$

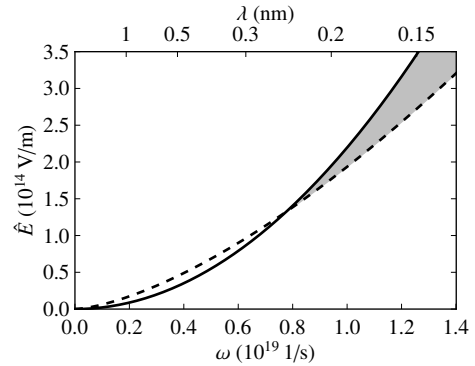


FIG. 6: Laser parameters for which a full spin flip is feasible (gray shaded area). The upper and lower bounds are given by (62) assuming that the electron can stay for $\mathcal{N} = 5000$ laser cycles in the electromagnetic field's focus.

The lower bound follows from $\mathcal{N} > \omega/(2\Omega)$ and the upper bound from (61a). For the lower limit we made the rather pessimistic assumption that a full spin flip would be required to detect a change of the spin orientation. More sensitive electron-spin measurements would allow to employ shorter laser pulses and/or lower intensities to verify the predicted effect. Furthermore, the inequalities in (62) implicate that an increase of the laser's wavelength may also require an increase of interaction time in terms of laser cycles \mathcal{N} . This is because when the wavelength λ is increased but all other parameters remain fixed, then the lower bound will finally exceed the upper bound of (62) and then the effect becomes unverifiable. Thus, there is a specific range of wavelengths and electric field strengths that render a full spin flip possible that depends on the parameter \mathcal{N} as illustrated in Fig. 6.

6. Conclusions

We investigated electron motion in two counterpropagating elliptically polarized laser waves of opposite helicity and found

spin precession around the laser waves' propagation axis. The spin precession is caused by the coupling of the light's spin density to the electron's spin degree of freedom. This mechanism is of similar origin as spin-orbit coupling. The spin-precession frequency is directly proportional to the product of the laser's intensity and the electromagnetic field's spin density. The observation of the predicted spin precession may become feasible by employing near-future high-intensity x-ray laser facilities. Furthermore, it might be interesting to generalize the setup considering electron-vortex beams [31] and/or light-vortex beams and to study a possible interaction of the light's spin or its orbital angular momentum with the electron beam's orbital angular momentum.

Acknowledgments

S. A. acknowledges the nice hospitality during his visit at Illinois State University. This work was supported by the NSF (USA).

-
- [1] M. Altarelli, R. Brinkmann, M. Chergui, W. Decking, B. Dobson, S. Düsterer, G. Grübel, W. Graeff, H. Graafsma, J. Hajdu *et al.*, eds., *The European X-Ray Free-Electron Laser Technical design report* (DESY XFEL Project Group European XFEL Project Team Deutsches Elektronen-Synchrotron Member of the Helmholtz Association, Hamburg, 2007).
 - [2] V. Yanovsky, V. Chvykov, G. Kalinchenko, P. Rousseau, T. Planchon, T. Matsuoka, A. Maksimchuk, J. Nees, G. Cheriaux, G. Mourou *et al.*, *Opt. Express* **16**, 2109 (2008).
 - [3] B. W. J. McNeil and N. R. Thompson, *Nat. Photonics* **4**, 814 (2010).
 - [4] P. Emma, R. Akre, J. Arthur, R. Bionta, C. Bostedt, J. Bozek, A. Brachmann, P. Bucksbaum, R. Coffee, F.-J. Decker *et al.*, *Nat. Photonics* **4**, 641 (2010).
 - [5] G. Mourou and T. Tajima, *Science* **331**, 41 (2011).
 - [6] G. Mourou, N. Fisch, V. Malkin, Z. Toroker, E. Khazanov, A. Sergeev, T. Tajima, and B. Le Garrec, *Opt. Commun.* **285**, 720 (2012).
 - [7] T. Brabec, ed., *Strong Field Laser Physics*, Springer Series in Optical Sciences, Vol. 134 (Springer, Heidelberg, 2008).
 - [8] F. Ehlotzky, K. Krajewska, and J. Z. Kamiński, *Rep. Prog. Phys.* **72**, 046401 (2009).
 - [9] A. Di Piazza, C. Müller, K. Z. Hatsagortsyan, and C. H. Keitel, *Rev. Mod. Phys.* **84**, 1177 (2012).
 - [10] M. W. Walser, D. J. Urbach, K. Z. Hatsagortsyan, S. X. Hu, and C. H. Keitel, *Phys. Rev. A* **65**, 043410 (2002).
 - [11] S. Ahrens, H. Bauke, C. H. Keitel, and C. Müller, *Phys. Rev. Lett.* **109**, 043601 (2012).
 - [12] S. Ahrens, H. Bauke, C. H. Keitel, and C. Müller, *Phys. Rev. A* **88**, 012115 (2013).
 - [13] H. Bauke, S. Ahrens, C. H. Keitel, and R. Grobe, *New J. Phys.* **16**, 103028 (2014).
 - [14] L. Zhang and Q. Niu, *Phys. Rev. Lett.* **112**, 085503 (2014).
 - [15] P. K. Mondal, B. Deb, and S. Majumder, *Phys. Rev. A* **89**, 063418 (2014).
 - [16] R. Beth, *Phys. Rev.* **50**, 115 (1936).
 - [17] J. D. Jackson, *Classical Electrodynamics* (John Wiley & Sons, New York, 1998).
 - [18] A. M. Stewart, *J. Mod. Opt.* **52**, 1145 (2005).
 - [19] S. M. Barnett, *J. Opt. (Bristol, U. K.)* **13**, 064010 (2011).
 - [20] R. P. Cameron and S. M. Barnett, *New J. Phys.* **14**, 123019 (2012).
 - [21] K. Y. Bliokh, A. Y. Bekshaev, and F. Nori, *New J. Phys.* **15**, 033026 (2013).
 - [22] S. M. Barnett, *Journal of Modern Optics* **57**, 1339 (2010).
 - [23] R. P. Cameron, *J. Opt.* **16**, 015708 (2014).
 - [24] F. Gross, *Relativistic Quantum Mechanics and Field Theory* (Wiley-VCH, Weinheim, 2004).
 - [25] B. Thaller, *Advanced Visual Quantum Mechanics* (Springer, Heidelberg, 2005).
 - [26] L. L. Foldy and S. A. Wouthuysen, *Phys. Rev.* **78**, 29 (1950).
 - [27] E. de Vries, *Fortschr. Phys.* **18**, 149 (1970).
 - [28] J. Fröhlich and U. Studer, *Rev. Mod. Phys.* **65**, 733 (1993).
 - [29] C. J. Joachain, N. J. Kylstra, and R. M. Potvliege, *Atoms in Intense Laser Fields* (Cambridge University Press, Cambridge, 2011).
 - [30] S. Ahrens, *Investigation of the Kapitza-Dirac effect in the relativistic regime*, Ph.D. thesis, Ruprecht-Karls Universität Heidelberg (2012), <http://www.ub.uni-heidelberg.de/archiv/14049>.
 - [31] A. G. Hayrapetyan, O. Matula, A. Aiello, A. Surzhykov, and S. Fritzsche, *Phys. Rev. Lett.* **112**, 134801 (2014).